Bis-μ-Oxo and μ-η^2:η^2-Peroxo Dicopper Complexes Studied within (Time-Dependent) Density-Functional and Many-Body Perturbation Theory

M. Rohrmüller,[a]* S. Herres-Pawlis,[b] M. Witte,[a] and W. G. Schmidt[a]

Based on the equilibrium geometries of $[Cu_2(dbdmed)_2O_2]^{2+}$ and $[Cu_2(en)_2O_2]^{2+}$ obtained within density-functional theory, we investigate their molecular electronic structure and optical response. Thereby results from occupation-constrained as well as time-dependent DFT (ΔSCF and TDDFT) are compared with Green's function-based approaches within many-body perturbation theory such as the GW approximation (GWA) to the quasiparticle energies and the Bethe-Salpeter equation (BSE) approach to the optical absorption. Concerning the ground-state energies and geometries, no clear trend with respect to the amount of exact exchange in the DFT calculations is found, and a strong dependence on the basis sets is to be noted. They affect the energy difference between bis-μ-oxo and μ-η^2:η^2-peroxo complexes by as much as 0.8 eV (18 kcal/mol). Even stronger, up to 5 eV is the influence of the exchange-correlation functional on the gap values obtained from the Kohn-Sham eigenvalues. Not only the value itself but also the trends observed upon the bis-μ-oxo to μ-η^2:η^2-peroxo transition are affected. In contrast, excitation energies obtained from ΔSCF and TDDFT are comparatively robust with respect to the details of the calculations. Noteworthy, in particular, is the near quantitative agreement between TDDFT and GWA+BSE for the optical spectra of $[Cu_2(en)_2O_2]^{2+}$. © 2013 Wiley Periodicals, Inc.

DOI: 10.1002/jcc.23230

Introduction

There is no need to emphasize the importance of copper enzymes. In particular, enzymes featuring a binuclear copper active site are receiving attention. The reactivity of the binuclear copper enzyme tyrosinase is impressive, as it not only reversibly binds O_2 through a side-on peroxide (μ-η^2:η^2-peroxo-dicopper(II)) but also hydroxylates phenols to catechols.[1,2] Each Cu(II) center in oxygenated tyrosinase is ligated by three imidazole nitrogen ligands, albeit one of the ligands is only weakly associated.[2,3] Extensive biomimetic inorganic model studies for this system have shown that Cu(I) can activate O_2 and bind O_2^{2-} in several different isoelectronic structural compositions (Fig. 1).[1,4–7] While nature chooses the side-on peroxo binding mode,[8–10] Cu(I) complexes can also bind peroxide in a $\mu(1,2\text{-}O_2^{2-})$ "end-on" fashion to generate a trans-$Cu_2^{II}(\mu\text{-}O_2^{2-})$ species.[11] Another feasible Cu_2O_2 structure is related to the μ-η^2:η^2 side-on form but comprises a fully cleaved O—O bond producing a formal $Cu_2^{III}(\mu\text{-}O^{2-})_2$ species, first discovered by Tolman and coworkers and now well established in many different ligand systems.[12–14]

Their detailed understanding and computational modeling are still major challenges. In this context, the structural and electronic properties of the μ-η^2:η^2-peroxo dicopper(II) and the bis-μ-oxo-dicopper(III) dimers (referred to as P and O in the following) are intensively investigated experimentally as well as computationally.[6] In spite of many efforts, the equilibrium between P and O cores is still regarded as a "torture track" for computation.[15] Very large variations in the predicted relative stabilities of P and O core motifs have been reported. The situation appears confusing since (i) different levels of theory are used in the calculations and (ii) the chemical equilibrium and properties of the μ-η^2:η^2-peroxo dicopper(II)- and the bis-μ-oxo-dicopper(III) dimers depends sensitively on the ligands, the solvent, and the counterions.

Many calculations in this context[15–19] use the density-functional theory (DFT) with either local (pure) functionals such as the generalized gradient approximation (GGA) or hybrid functionals such as B3LYP[20–32] to describe the electron exchange and correlation (XC) energy. The application of DFT to systems such as structure P which is thought to represent a magnetic coupling case—where a closed shell determinant does not provide a good description of the electronic structure—appears questionable at first sight. However, Liakos and Neese[33] argue that P is so strongly coupled that it is outside the magnetic coupling regime, and treatments starting from a closed shell determinant are adequate. Although DFT is generally believed to result in reliable structures and energies in bioinorganic chemistry[34]—with some arguments concerning the accuracy of GGA vs. functionals that contain some amount of Hartree-Fock exchange[15,18,19,21,22,30,35]—occasionally remarkable differences with respect to the wave function based methods

[a] M. Rohrmüller, M. Witte, W. G. Schmidt
Lehrstuhl für Theoretische Physik, Universität Paderborn, 33098 Paderborn, Germany
E-mail: martin.rohrmueller@upb.de
[b] S. Herres-Pawlis
Department Chemie, Ludwig-Maximilians-Universität München, Butenandtstr. 5-13, 81377 München, Germany

Contract/grant sponsor: Deutsche Forschungsgemeinschaft; Contract/grant number: FOR1405.

© 2013 Wiley Periodicals, Inc.

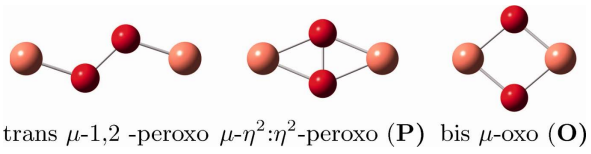

Figure 1. The three most common structures of the $Cu_2O_2^{2+}$ core. [Color figure can be viewed in the online issue, which is available at wileyonlinelibrary.com.]

are reported. Calculations on multireference second-order perturbation theory level (CASPT2) predict O to be more stable by about 0.55 eV (12.7 kcal/mol) whereas B3LYP favors P by about 0.86 eV (19.8 kcal/mol) in the simplest case, where each copper atom is supported by three ammonia ligands.[36] However, one difficulty in this context is that methods like CASPT2 are limited to rather small systems, which can be quite different from the systems of actual interest. When somewhat larger systems are treated, compromises often have to be made that may in fact lead to wrong conclusions about the accuracy of DFT.[37] In an extensive comparative study, Cramer et al.[15] found energy difference of several eV for various flavors of DFT and wave function methods. They concluded from their extensive comparison of experimental data with computational results that DFT calculations using local functionals for the XC energy are the method of choice for the Cu_2O_2 system, especially if larger ligands are to be modeled that render the otherwise quantitatively similar completely renormalized coupled cluster (CR-CC) multireference configuration interaction less practical for computational reasons. Gherman and Cramer[19] studied in a more recent review the reliability of various flavors of pure and hybrid XC functionals for the description of molecules containing a $Cu_2O_2^{2+}$ core and found that different functionals are required for accuracy in different regions of the potential energy surface and that sometimes results obtained with small ligands can be reasonably applied to larger ones. The results by Cramer et al. on the transition between P and O core presented in Ref. [15] were obtained for the simplest possible model system consisting of the Cu_2O_2 core and four or six ammonia molecules. Due to the truncated ligands, the study is primarily of methodological value. In fact, no real transition state was found but rather a general bias towards the P core and a curve progression without maximum. Liakos and Neese[33] recently studied $[Cu_2(en)_2O_2]^{2+}$ oxo (O1) and peroxo (P1) as the simplest type of dicopper core with saturated neutral amine ligands that avoids the complication associated with the use of ammonia (artificial hydrogen bonds, too much coordinative flexibility). It contains simply ethylene diamine (en) as a capping ligand, cf. Figure 2.

On the local-pair natural orbital coupled cluster (LPNO-CCSD) level of theory including relativistic and solvent effects, the O1 isomer was found to be slightly more stable than the P1 structure. Performing DFT calculations, Liakos and Neese found that the energetics depend strongly on the fraction of exact exchange (EEX) included in the calculations. In fact, the O1 P1 energy difference is almost linearly related to the fraction of EEX used. Among the functionals investigated, B3LYP and B1LYP were in best agreement with the LPNO-CCSD results. Neese et al.[38] also noticed a strong influence of relativistic effects on the potential-energy surface. Due to the ligand truncation in simplified models chelate effects can often not be taken into account which implies heavy deviations in comparison to the "real" complex models.[32]

As discussed above, the existing calculations, mainly based on DFT, provide no unambiguous picture concerning the structure and energetics of a P and O system, although generally, ground-state properties tend to be described quite reliably within DFT, see, e.g., Ref. [34]. The situation is even more complicated for excited-state properties. Since the foundations of DFT restrict it to ground states, the calculation of excited states and their properties requires extensions to DFT. The large majority of neutral molecular excitations is presently calculated using the linear-response approach to time-dependent DFT (TDDFT). While this approach is in principle well-founded, see, e.g., Ref. [39], its practical application typically rests on the adiabatic approximation and is plagued with the well-known shortcomings of the XC functionals used in the implementation. In particular, states that have ionic or charge transfer character are predicted rather poorly, with errors which may exceed 1–2 eV.[34] Much progress in this respect has recently been made using range-separated hybrid functionals.[34,40,41]. An alternative to TDDFT is to performed separate self-consistent-field (SCF) calculations for each state of interest (occupation-constrained or ΔSCF approach), cf., e.g., Refs. [42–45]. However, this approach is computationally laborious since it requires potentially many SCF calculations and the orthogonality of ground and excited states is not guaranteed. In addition, similar to TDDFT, ΔSCF calculations suffer from the limitations inherent to the presently available XC functionals. A completely different type of methods to calculate excited-state properties is referred to as propagator or Green's function approaches.[39] At least in principle these methods are not plagued by the shortcomings of the XC functionals used within DFT. They start from the screening response of the electronic system after electronic or optical excitation. Accordingly, the dynamically screened or shielded Coulomb interaction W is the central quantity used in these methods. The excitation energies correspond to the poles of single- and two-particle Green's functions that are obtained by means of many-body perturbation theory. By evaluating the one-electron Green's function G, single-particle excitations, e.g., ionization energies and electron affinities, are derived that can be measured in photoemission and inverse photoemission spectroscopies. Two-particle Green's functions of the electronic system allow to access electron-hole pair energies and collective excitations,

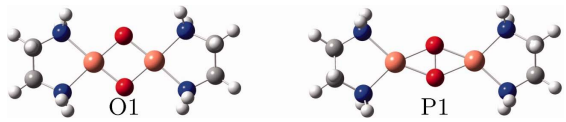

Figure 2. Relaxed geometries (DFT-GGA) of $[Cu_2(en)_2O_2]^{2+}$ oxo (O1) and peroxo (P1) configuration. Copper, oxygen, nitrogen, carbon, and hydrogen are gray (orange) core, dark (red) core, dark (blue) ligand, gray ligand, and white atoms. [Color figure can be viewed in the online issue, which is available at wileyonlinelibrary.com.]

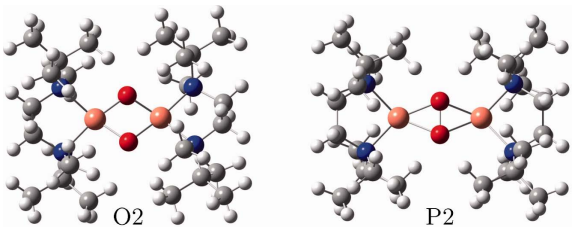

Figure 3. Relaxed geometries (DFT-GGA) of $[Cu_2(dbdmed)_2O_2]^{2+}$. Copper, oxygen, nitrogen, carbon, and hydrogen are gray (orange) core, dark (red) core, dark (blue) ligand, gray ligand, and white atoms. [Color figure can be viewed in the online issue, which is available at wileyonlinelibrary.com.]

e.g., plasmons. In the practical implementation, one resorts to approximations to describe the most relevant correlation mechanisms. Hedin's so-called GW approach,[46,47] which represents a linear expansion of the XC self-energy operator Σ of the electrons in the screened potential W instead of the bare Coulomb potential (which gives only the exchange interaction), is the most widely used approximation in this context. This scheme allows for deriving a single-quasiparticle (QP) equation of a structure similar to the Kohn-Sham equation used in the DFT.[48] Only the (semi-)local potential V^{XC} is replaced by the XC self-energy operator Σ. This suggests to calculate QP bands by using a first-order perturbative approach with respect to $(\Sigma - V^{XC})$.[49–51] However, QP transition energies do in general not correctly describe optical excitation energies, i.e., photon absorption processes. The interaction of electron-hole pairs may dramatically shift the peak positions as well as appreciably distort the spectral lineshape. The electron-hole interaction is accounted for by solving the Bethe-Salpeter equation (BSE) for the polarization function.[52,53] Starting from DFT calculations, it has become possible to solve the BSE from *first principles*. Optical spectra including the effects of electron-hole interaction were obtained for a series of bulk semiconductors and insulators[54–56] and their surfaces[57,58] as well as molecular systems.[44,59–69] The formalism has been generalized also for the calculation of nonlinear optical spectra.[70,71]

In the present study, the reliability and predictive power of DFT-based methods with respect to the ground- and excited-state properties of bis-μ-oxo and μ-η^2:η^2-peroxo dicopper complexes is evaluated. To this end, we perform (occupation-constrained, time-dependent) DFT calculations of two prototypical model complexes $[Cu_2(en)_2O_2]^{2+}$ (O1, P1) and $[Cu_2(dbdmed)_2O_2]^{2+}$ (O2, P2) shown in the Figures 2 and 3, respectively. Thereby both (semi)local (PW91[72]) as well as hybrid (HSE06[73], B3LYP[74–76]) and long-range corrected (CAM-B3LYP[77]) XC functionals are probed. In order to assess the sensitivity of the results on the basis set, we employ a plane-wave basis in addition to the localized 6-31g(d) and cc-pVDZ basis sets. Plane waves form, by construction, a complete and orthogonal basis set for which the numerical convergence can be reliably controlled. They do not suffer from the limitations necessarily accompanying basis sets consisting of a finite number of localized atom-centered functions such as the basis set superposition error. On the other hand, they require periodic boundary conditions which increases the computational load in particular for single molecules that need to be embedded in large vacuum regions. In case of O1 and P1, the results of TDDFT for electronic and optical excitations are compared with the outcome of the Green's function approaches GW and BSE.

Methodology

Ground-state properties

Ground-state total-energy and electronic-structure calculations are performed using the Vienna *Ab-initio* Simulation Package (VASP)[78] and Gaussian09[79] implementation of the DFT. In the VASP calculations, the electron-ion interaction is described by the projector augmented-wave (PAW) method,[80,81] and the valence wave functions are expanded into plane waves up to an energy cutoff of 400 eV. A supercell of up to $28\times28\times28$ Å^3 is used. Within the unit cell, the molecules are positioned such that the lateral interactions have been minimized. All energetic quantities are extrapolated to infinite cell size to eliminate the higher order charge density interactions. Test calculations show that the energy eigenvalues are converged within a few hundredths of an eV. The calculations with Gaussian09 are all-electron with tightened criterion for electronic and geometric convergence. Thereby 6-31g(d) and cc-pVDZ basis sets were used. In addition, we performed convergence tests using double and triple-ζ basis sets.

In order to assess the possible influence of the solvent on the molecular optical response, we performed—in addition to calculations where the solvent molecules were explicitly taken in account—continuum model simulations. Thereby we used on the one hand the integral equation formalism[82] within the polarizable continuum model implemented in Gaussian09, with standard UFF atomic radii scaled by 1.1 to generate the cavity and an average of 5.0 integration points per Å^2. On the other hand, for the case of plane-wave calculations, we implemented a modified version of the continuum solvation model proposed by Fattebert and Gygi[83] which is based on a new density functional that includes the electrostatic effects of a dielectric continuum by means of a dielectric function that depends on the electronic density ρ of the solute. Specifically, we use the smoothly varying ε function proposed in Ref. [84].

$$\epsilon[\rho(\vec{r})] = \begin{cases} 1 & \rho > \rho_{\max} \\ \exp(t(\ln(\rho))) & \rho_{\min} < \rho < \rho_{\max} \\ \epsilon_\infty & \rho < \rho_{\min} \end{cases} \quad (1)$$

where ε_∞ equals the permittivity of the solvent in absence of the solvate, and $\rho_{\min}$ and $\rho_{\max}$ are set to 0.00067 and 0.01012 e/Å^3, respectively. Here $t(x)$ is a general, smooth function that decreases monotonically from $t(\ln\ \rho_{\min})=\ln\ \varepsilon_\infty$ to $t(\ln\ \rho_{\max})=0$ which we adopt from Ref. [84]. We determine the solute's electronic structure in a perturbative manner, where the Kohn-Sham Hamiltonian is augmented by the additional potential term

$$V_\epsilon = -\frac{1}{8\pi}\frac{1}{\epsilon([\rho(\vec{r})])^2}\left|\vec{\nabla}V^{H}\right|^2\frac{d\epsilon}{d\rho}(\vec{r}). \quad (2)$$

where V^H denotes the Hartree potential.

Electronic excitations

DFT calculations typically considerably underestimate electronic excitation energies[39]. Reliable QP gaps and exciton pair energies for molecules and clusters, however, can be obtained from occupation constraint DFT methods. Thereby the QP gap is obtained directly as difference between the ionization energy (IE) and electron affinity (EA)

$$E_g^{QP} = E(N+1,\vec{R}) + E(N-1,\vec{R}) - 2E(N,\vec{R}), \tag{3}$$

where $E(N,\vec{R})$, $E(N+1,\vec{R})$, and $E(N-1,\vec{R})$ represent the energy of a N, $N+1$, and $N-1$ electron system, respectively, with the equilibrium geometry $\vec{R}$ of the N electron system. Alternatively, according to Janak's Theorem (see, e.g., Ref. [42]), the ionization energy (electron affinity) can be calculated as the eigenvalue of the former highest occupied molecular orbital, HOMO (lowest unoccupied molecular orbital, LUMO) occupied with a half electron IE $= \varepsilon^{IE}_{HOMO,0.5}$ (EA $= \varepsilon^{EA}_{LUMO,0.5}$). Therefore the QP gap is also obtained from

$$E_g^{QP} = \varepsilon^{EA}_{LUMO,\,0.5} - \varepsilon^{IE}_{HOMO,\,0.5}. \tag{4}$$

The systematic failure of ΔSCF calculations is of the same order as the ground-state energy calculations and depends essentially on the accuracy of the extrapolation to infinite cell size for the charged super cell. Typical error bars are below 0.1 eV. For the molecules, the obtained QP gaps E_g^{QP} are compared to the gap E_g^{G0W0} that has been obtained from the GW approximation (GWA) to the electronic self-energy. Thereby we perform perturbative, one-shot G_0W_0 calculations based on the single particle orbitals and eigenvalues obtained from the preceding DFT calculation.

Thereby we use the implementation described in Ref. [85]. A cutoff of 100 eV for the response function and 128 frequency points are used. The maximum cell size for GW calculations is $12.5\times14\times20$ Å^3 which mimics a vacuum of 10 Å in every direction around the ion. Test calculations with varying cell sizes indicate an error bar of about 0.1 eV that has to be attributed to the periodic boundary conditions.

Optical spectra

Optical absorption spectra are calculated using the linear-response approach to TDDFT including the adiabatic approximation for the XC kernel as implemented in Gaussian09.[79,86,87] In order to gain more insight into the relation between molecular states and the optical response, the latter was also calculated within the independent-particle approximation[88–91] (IPA), which allows for a simple interpretation of the absorption peaks in terms of transitions between single-particle states. On the other hand, Bethe-Salpeter-type calculations were performed for O1 and P1, in order assess the predictive power of TDDFT for μ-η^2:η^2-peroxo dicopper(II)-and the bis-μ-oxo-dicopper (III) dimers. In order to allow for comparison with experimental data, we average over the three Cartesian directions

$$\epsilon(\hbar\omega) = \frac{1}{3}\sum_{i=x,y,z}\epsilon_{ii}(\hbar\omega). \tag{5}$$

The dielectric function within the IPA or by solving the BSE is based on the electronic structure as obtained from either the DFT calculations or from the GWA.

Solving the BSE includes the electron-hole attraction and local-field effects in the dielectric function. For practical calculations, the BSE is transformed into a two-particle Schrödinger equation. The resonant part of the exciton Hamiltonian[92] (Tamm-Dancoff approximation, BSE-TDA) is given by

$$\begin{aligned} H_{vc,v'c'} &= (\epsilon_c - \epsilon_v)\delta_{vv'}\delta_{cc'} \\ &+ 2\int\int d\mathbf{r}d\mathbf{r}'\psi_c^*(\mathbf{r})\psi_v(\mathbf{r})\bar{v}(\mathbf{r}-\mathbf{r}')\psi_{c'}(\mathbf{r}')\psi_{v'}^*(\mathbf{r}') \\ &- \int\int d\mathbf{r}d\mathbf{r}'\psi_c^*(\mathbf{r})\psi_{c'}(\mathbf{r})W(\mathbf{r},\mathbf{r}')\psi_v(\mathbf{r}')\psi_{v'}^*(\mathbf{r}'). \end{aligned} \tag{6}$$

It describes the interaction of pairs of electrons in conduction states $|c\rangle$ and holes in valence states $|v\rangle$. The diagonal first part is given by the QP energies obtained in GWA. Again perturbative, one-shot G_0W_0 calculations are used here. The second, the electron-hole exchange term, where the short-range part of the bare Coulomb potential $\bar{v}$ enters, reflects the influence of local fields. Finally, the third part, which describes the screened electron-hole attraction, is calculated using a model dielectric function as proposed by Bechstedt *et al*.[49] In order to account for the molecular charge-density inhomogeneities, we use state-dependent electron densities which were calculated using the mean-density approximation

$$\rho_n = \int d\mathbf{r}^3\rho(\mathbf{r})|\psi_n(\mathbf{r})|^2, \tag{7}$$

as input in the model dielectric function. This approach accounts approximately for the effects of local fields on the screening. The model dielectric function, which reduces the computational effort substantially, depends on the static dielectric constant ε_∞. In case of inorganic semiconductors[56,93,94,95] as well as molecular crystals[44,60] the application of this model dielectric function leads to rather accurate results. This is related to the fact that the model dielectric function depends on the local charge density and therefore carries information about the local screening. In the case of molecular excitations, the correct choice of ε_∞ is difficult. The authors of Ref. [96] defined an effective molecular volume in order to address this problem in their optical response calculation of poly-para-phenylenevinylene. In the present calculations, ε_∞ has been obtained from an iterative procedure. Thereby it is required that the main optical peaks obtained within the BSE approach agree energetically with the corresponding transitions obtained from the ΔSCF method. This procedure results in an effective screening constant of $\varepsilon_\infty = 1.85$ and allows for determining an error bar of the order of about 0.2 eV for the peak positions obtained from the Bethe-Salpeter approach.

The dimension of the exciton Hamiltonian (eq. 6) is determined by the size of the energy window for conduction and valence states. Here, we include states of Kohn-Sham eigenvalues which satisfy $\varepsilon_c(k) - \varepsilon_v(k) < 20$ eV. For the actual calculation of the spectra, we use the time-evolution algorithm proposed by one of the present authors.[53]

Table 1. Key bond lengths and relative energies for both O and P singlet cores of $[Cu_2(en)_2O_2]^{2+}$ (O1, P1) and $[Cu_2(dbdmed)_2\ O_2]^{2+}$ (O2, P2) calculated with different basis sets and XC functionals.

Configuration	Functional	Basis	O-O [Å]	Cu-Cu [Å]	Cu-N [Å]	$\Delta\ E_{sing\ -\ trip}$ [eV]	$\Delta\ E_{O\ -\ P}$ [eV]
O1	PW91	cc-pVDZ	2.341	2.769	1.971	−0.57	−0.25
O1	B3LYP	cc-pVDZ	2.319	2.753	1.976	−0.71	0.03
O1	CAM-B3LYP	cc-pVDZ	2.296	2.713	1.949	−0.36	0.01
O2	PW91	6–31g(d)	2.270	2.810	1.980, 1.986	−0.90	–
O2	PW91	cc-pVDZ	2.306	2.870	2.043, 2.041	−0.69	−0.17
O2	PW91	pw	2.240	2.890	2.054, 2.060	−0.97	0.21
O2	B3LYP	6–31g(d)	2.257	2.788	1.999, 1.995	−0.85	−0.51
O2	B3LYP	cc-pVDZ	2.261	2.862	2.046, 2.058	−0.67	0.22
O2	HSE06	6–31g(d)	2.255	2.753	1.973, 1.970	−0.85	−0.55
O2	HSE06	cc-pVDZ	2.260	2.819	2.026, 2.016	−0.42	0.21
O2	CAM-B3LYP	cc-pVDZ	2.242	2.812	2.018, 2.021	−0.88	0.19
P1	PW91	cc-pVDZ	1.498	3.549	2.008	−0.38	
P1	B3LYP	cc-pVDZ	1.448	3.585	2.023	0.13	
P1	CAM-B3LYP	cc-pVDZ	1.413	3.561	2.004	0.41	
P2	PW91	6–31g(d)	–	–	–	–	
P2	PW91	cc-pVDZ	1.498	3.613	2.039	−0.43	
P2	PW91	pw	1.495	3.585	2.042, 2.038	−1.12	
P2	B3LYP	6–31g(d)	1.491	3.481	1.991	0.07	
P2	B3LYP	cc-pvDZ	1.451	3.630	2.050	0.08	
P2	HSE06	6–31g(d)	1.463	3.459	1.971	0.25	
P2	HSE06	cc-pVDZ	1.429	3.603	2.026	0.22	
P2	CAM-B3LYP	cc-pVDZ	1.462	3.437	1.971	0.44	

Recent results[62,63,66,97] question the validity of the TDA for molecular systems. Therefore, in addition to BSE-TDA, calculations with the full exciton Hamiltonian were also performed (BSE).

Results and Discussion

Structure and energetics

Ground-state geometries and energies for both O, P cores of $[Cu_2(en)_2O_2]^{2+}$ (O1, P1) and $[Cu_2(dbdmed)_2O_2]^{2+}$ (O2, P2) were calculated starting from both singlet and triplet spin states as well as enforcing C_1 symmetry or without symmetry constraints. Thereby various XC functionals and basis sets were used. The key geometrical parameters of singlet states and energy differences are summarized in Table 1.

Concerning the symmetry, P2 singlet with an inversion symmetric core turns out be less favored (by at most 0.4 eV/9 kcal/mol within CAM-B3LYP and cc-pVDZ) than the corresponding C_1 calculations for triplet states. The geometry of P2 triplet cores is not planar. Rather, a butterfly angle of up to 53° (within PW91 and cc-pVDZ) is observed. For O2 triplet, this effect is nearly vanishing (max. 2°). O and P singlet states, on the other hand, are found to have always a planar core geometry.

The spin singlet configuration is clearly preferred for O2. Irrespective of the XC functional used and for all basis sets, a clear energetical separation between at most 0.97 eV (22 kcal/mol, PW91, and plane waves) and at least 0.42 eV (10 kcal/mol, HSE06, and cc-pVDZ) is obtained. Concluding from the ground-state energies, the situation seems less clear for the P2 structure. While both the plane-wave implementation of PW91 as well as using a cc-pVDZ basis in conjunction with the semi-local XC functional indicate a strong preference (by 1.12 eV/26 kcal/mol and 0.43 eV/10 kcal/mol, respectively) for the singlet state, the picture changes as soon as a fraction of EEX is included in the calculations. In particular, the HSE06 and CAM-B3LYP results favor the spin triplet state. This is in line with the above discussion for O2, where the singlet was least favored in case of HSE06 calculations. The same energy trend is also seen in our calculations for O1 and P1: The EEX contribution in the XC functional reduces or even inverts the energetical preference of the spin singlet state. However, as we will discuss below, the calculated optical signatures clearly speak in favor of spin singlets both for O and P. Therefore, we will restrict the discussion to spin singlet systems in the following.

With respect to the equilibrium between O and P cores, the present results clearly show a dependence on the XC functional used in the calculations. In case of $[Cu_2(en)_2O_2]^{2+}$, plane wave PW91 (cc-pVDZ) calculations favor O1 by 0.25 eV (6 kcal/mol), while B3LYP (cc-pVDZ) find P1 to be more stable by 0.03 eV (0.7 kcal/mol). This trend agrees with recent findings in Ref. [33], where the energetical preference of P over O was found to scale with the EEX amount in the XC functional. Ambiguous results are obtained for $[Cu_2(dbdmed)_2O_2]^{2+}$. The O2 structure is clearly favored when the hybrid functionals B3LYP or HSE06 are combined with a 6-31g(d) basis. In this case, it is 0.51 eV (12 kcal/mol) or even 0.55 eV (13 kcal/mol) more stable than P2. Plane-wave calculation with PW91, on the other hand, favors P2 over O2 structure by 0.21 eV (5 kcal/mol). We mention that the combination of a 6-31g(d) basis with the PW91 functional did not result in a stable P2 configuration. The numbers in Table 1 for $[Cu_2(dbdmed)_2O_2]^{2+}$ indicate a remarkable influence of the basis set. If one considers the 6-31g(d) calculations, hybrid functionals seem to stabilize O2. If, on the

Table 2. Kohn-Sham HOMO LUMO gaps of $[Cu_2(en)_2O_2]^{2+}$ (O1, P1) and $[Cu_2(dbdmed)_2O_2]^{2+}$ (O2, P2), without and with inversion symmetry (C_1, C_i).

Configuration	Functional	Basis	E_g^{C1} [eV]	E_g^{Ci} [eV]
O1	PW91	cc-pVDZ	0.92	
O1	PW91	pw	0.99	
O1	B3LYP	cc-pVDZ	3.26	
O1	CAM-B3LYP	cc-pVDZ	6.55	
O2	PW91	6–31g(d)	1.19	1.19
O2	PW91	cc-pVDZ	1.00	1.00
O2	PW91	pw	1.04	
O2	B3LYP	6–31g(d)	3.46	3.45
O2	B3LYP	cc-pVDZ	3.19	3.19
O2	HSE06	6–31g(d)	3.28	3.27
O2	HSE06	cc-pVDZ	2.99	2.99
O2	CAM-B3LYP	cc-pVDZ	6.08	
P1	PW91	cc-pVDZ	1.15	
P1	PW91	pw	1.09	
P1	B3LYP	cc-pVDZ	2.83	
P1	CAM-B3LYP	cc-pVDZ	5.25	
P2	PW91	6–31g(d)	–	–
P2	PW91	cc-pVDZ	1.29	1.25
P2	PW91	pw	1.36	
P2	B3LYP	6–31g(d)	2.60	2.59
P2	B3LYP	cc-pVDZ	2.35	2.34
P2	HSE06	6–31g(d)	2.27	2.25
P2	HSE06	cc-pVDZ	2.01	2.00
P2	CAM-B3LYP	cc-pVDZ	4.49	

other hand, the cc-pVDZ data are selected, it seems as if an increased amount of EEX reduces the P2 energy with respect to the O2 data. The latter trend agrees with the cc-pVDZ data obtained for $[Cu_2(en)_2O_2]^{2+}$ (O1, P1).

The basis set also has a pronounced influence on the geometrical data. The Cu—Cu distance of O2 calculated using a 6-31g(d) basis is about 0.06…0.08 Å shorter than in the corresponding cc-pVDZ calculations using either PW91, B3LYP, or HSE06 to describe the electron exchange correlation. The largest Cu—Cu distance of 2.89 Å is obtained by combining PW91 with plane-wave calculations, whereas 2.75 Å—obtained using HSE06 together with 6-31g(d)—mark the lower limit. The influence of the XC functional is slightly smaller than the one found for the basis set. The hybrid functionals B3LYP and HSE06 tend to result in Cu—Cu distances that are about 0.01…0.05 Å shorter than the PW91 value. In case of P2, the Cu—Cu distance calculated with the 6-31g(d) basis is about 0.15 Å smaller than in the corresponding cc-pVDZ calculations. The variation across the PW91, B3LYP, and HSE06 results is fairly small, of the order of 0.03 Å. Only the CAM-B3LYP calculations give rise to a stronger deviation. They result in the shortest P2 Cu—Cu distance obtained in the present work of 3.44 Å. The upper limit of 3.63 Å is obtained with cc-pVDZ calculations within B3LYP. Altogether, the structural data calculated in the present study scatter around the values obtained in earlier works, e.g., the B3LYP study of Siegbahn.[21]

The trend that hybrid functionals result in general in larger Cu—Cu distances than obtained by the semilocal PW91 found for $[Cu_2(dbdmed)_2O_2]^{2+}$ does also hold for $[Cu_2(en)_2O_2]^{2+}$. Here, Cu—Cu distances of about 2.76 Å are calculated for O1. The P1 configuration is characterized by a distance of about 3.56 Å. This value agrees typically within 0.1 Å with the literature data, see, e.g., Ref. [33].

Electronic excitations

Starting from the relaxed geometries of O1, P1, O2, and P2 electronic key quantities were calculated. In Table 2, the single-particle gaps calculated from the differences of the Kohn-Sham eigenvalues using different XC functionals and basis sets are compiled. While the influence of the symmetry on the gap values is nearly negligible, we find a pronounced change upon O–P transition. It depends, however, on the XC functional and basis set used in the calculation. The semilocal PW91 functional in combination with plane waves leads to an increase of the gap value of 0.1 and 0.32 eV for the transition from O1 to P1 and O2 to P2, respectively. This trend holds also for cc-pVDZ calculations. The hybrid functionals B3LYP and HSE06 on the other hand find a reduction of the HOMO-LUMO gap of the order of 0.8…1.0 eV both for O1, P1 ($[Cu_2(en)_2O_2]^{2+}$) and O2, P2 ($[Cu_2(dbdmed)_2O_2]^{2+}$) irrespective of the basis set used. The largest gap values are obtained by combining CAM-B3LYP with the cc-pVDZ basis. In fact, the CAM-B3LYP results for O2 exceed the PW91 findings using the same cc-pVDZ basis by more than 5 eV. In general, the present results show the expected trend of an increase of the HUMO-LUMO transition energy by an increased amount of EEX contained in the XC functional. This trend is illustrated in Figure 4. The EXX contribution to the CAM-B3LYP functional varies from 19% for short-range interactions to 65% in the long-range part. However, not only the eigenvalues change upon variation of the XC-functional, also the energy ordering of the electronic states is affected as shown in Figure 5 for the case of O1 and P1. In the latter case, even the HOMO and LUMO are affected. Interestingly, the order of the highest occupied states is the same for PW91 and G_0W_0 calculations, whereas B3LYP and G_0W_0 agree concerning the order of the lowest unoccupied states. In general, the reordering is more pronounced for P1 than for O1 and in particular concerns the unoccupied states.

In Table 3, the ionization energies (IE) and electron affinities (EA) for O and P ions are compiled. In case of calculations with periodic boundary conditions, the respective energy

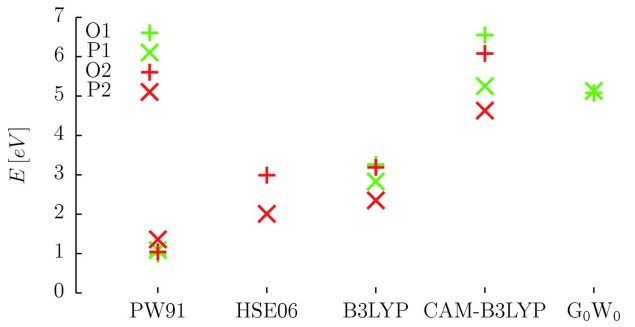

Figure 4. HOMO-LUMO gaps of $[Cu_2(en)_2O_2]^{2+}$ (O1, P1) and $[Cu_2(dbdmed)_2O_2]^{2+}$ (O2, P2) from HSE06, B3LYP, and CAM-B3LYP calculations with cc-pVDZ basis in comparison with plane-wave PW91 and G_0W_0 results. [Color figure can be viewed in the online issue, which is available at wileyonlinelibrary.com.]

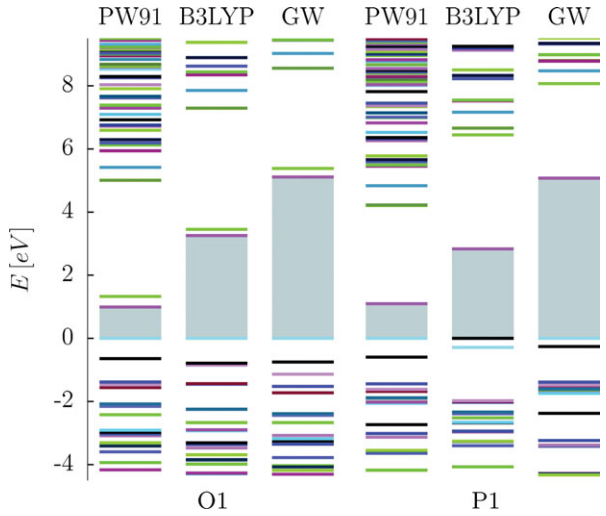

Figure 5. Molecular orbital spectra of $[Cu_2(en)_2O_2]^{2+}$ within different approximations. Same colors indicate electronic states of the same orbital character. The HOMO-LUMO gap is indicated gray.

differences were extrapolated to infinite super cell size, following the approach used in Ref. [66]. Compared to the HOMO-LUMO transition energies, we find the electron affinities and ionization energies to be relatively robust with respect to the XC functional and basis set used in the calculation. This holds also for the computational procedure itself: The Slater-Janak Transition-State (SJ-TS) values in Table 3 have been calculated using Janak's Theorem and are in very close agreement (within 0.06 eV) with the corresponding values obtained from differences in total energy. The ionization energies of the bis-μ-oxo structures O1 and O2 lie between 15.1…16.3 and 13.1…13.9 eV and are about 0.1…1.2 and 0.5…1.0 eV larger than the corresponding values for P1 and P2. The electron affinities of O1 and O2 of about 9 and 8 eV are typically about half an eV larger than the corresponding P1 and P2 values.

As discussed above, the ionization energies and electron affinities can be used to calculate QP gaps. The corresponding values, together with G_0W_0 results are compiled in Table 4. The influence of the basis set on the gap value is remarkably large, of the order of 0.5 eV. We find the gap value to reduce monotonically by going from the 6-31g(d) to the cc-pVDZ to the plane-wave basis. The XC functional used in the underlying DFT calculations is of similar importance for the result. However, in this case, no clear trend can be recognized. Remarkably close are the gap values derived from the ΔSCF and Janak-type calculations. While the QP gaps of the $[Cu_2(en)_2O_2]^{2+}$ species O1 and P1 are about one eV larger than the corresponding calculations for the $[Cu_2(dbdmed)_2O_2]^{2+}$ species O2 and P2, the scatter between the calculated gap values is too large to reliably state a trend concerning the gap change upon the bis-μ-oxo to μ-η^2:η^2-peroxo transition. The comparison of the gap values from Table 4 with the eigenvalue differences from Table 2 shows that the QP effects in the molecular species are of the order of about 4 eV.

Optical response

Based on the electronic structure obtained either within DFT or G_0W_0, the optical response of O1 and P1 ($[Cu_2(en)_2O_2]^{2+}$) is calculated. The corresponding IPA, TDDFT, and GW-BSE spectra are shown in Figure 6. On the IPA level of theory, one pronounced absorption peak at around 2.8/1.7 eV is observed for

Table 3. Ionisation energy (IE) and electron affinity (EA) of $[Cu_2(en)_2O_2]^{2+}$ (O1, P1) and $[Cu_2(dbdmed)_2O_2]^{2+}$ (O2, P2) calculated with different XC functionals and basis sets.

Configuration	Functional	Method	Basis	*IE* [eV]	*EA* [eV]
O1	PW91	ΔSCF	cc-pVDZ	15.47	9.03
O1	PW91	ΔSCF	pw	15.13	9.14
O1	B3LYP	ΔSCF	cc-pVDZ	15.95	9.18
O1	CAM-B3LYP	ΔSCF	cc-pVDZ	16.25	9.42
O2	PW91	ΔSCF	6–31g(d)	13.13	7.57
O2	PW91	ΔSCF	cc-pVDZ	13.21	8.07
O2	PW91	ΔSCF	pw	13.44	8.38
O2	PW91	SJ-TS	pw	13.38	8.41
O2	B3LYP	ΔSCF	6–31g(d)	13.81	7.94
O2	B3LYP	ΔSCF	cc-pVDZ	13.82	8.36
O2	HSE06	ΔSCF	6–31g(d)	13.89	7.97
O2	HSE06	ΔSCF	cc-pVDZ	13.91	8.52
P1	PW91	ΔSCF	cc-pVDZ	15.37	8.25
P1	PW91	ΔSCF	pw	14.75	8.12
P1	B3LYP	ΔSCF	cc-pVDZ	15.12	8.76
P1	CAM-B3LYP	ΔSCF	cc-pVDZ	15.05	8.98
P2	PW91	ΔSCF	6–31g(d)	–	–
P2	PW91	ΔSCF	cc-pVDZ	12.72	7.42
P2	PW91	ΔSCF	pw	12.63	7.55
P2	PW91	SJ-TS	pw	12.65	7.55
P2	B3LYP	ΔSCF	6–31g(d)	12.60	7.25
P2	B3LYP	ΔSCF	cc-pVDZ	12.93	8.02
P2	HSE06	ΔSCF	6–31g(d)	12.54	7.21
P2	HSE06	ΔSCF	cc-pVDZ	12.89	8.01

Table 4. Calculated quasiparticle gap of $[Cu_2(en)_2O_2]^{2+}$ (O1, P1) and $[Cu_2(dbdmed)_2O_2]^{2+}$ (O2, P2).

Configuration	Functional	Method	Basis	E^{QP} [eV]
O1	PW91	ΔSCF	cc-pVDZ	6.44
O1	PW91	ΔSCF	pw	5.98
O1	B3LYP	ΔSCF	cc-pVDZ	6.77
O1	CAM-B3LYP	ΔSCF	cc-pVDZ	6.82
O1	PW91	G_0W_0	pw	5.11
O2	PW91	ΔSCF	6–31g(d)	5.55
O2	PW91	ΔSCF	cc-pVDZ	5.14
O2	PW91	ΔSCF	pw	5.06
O2	PW91	SJ-TS	pw	4.97
O2	B3LYP	ΔSCF	6–31g(d)	5.87
O2	B3LYP	ΔSCF	cc-pVDZ	5.46
O2	HSE06	ΔSCF	6–31g(d)	5.92
O2	HSE06	ΔSCF	cc-pVDZ	5.39
P1	PW91	ΔSCF	cc-pVDZ	7.12
P1	PW91	ΔSCF	pw	6.63
P1	B3LYP	ΔSCF	cc-pVDZ	6.36
P1	CAM-B3LYP	ΔSCF	cc-pVDZ	6.54
P1	PW91	G_0W_0	pw	5.17
P2	PW91	ΔSCF	6–31g(d)	–
P2	PW91	ΔSCF	cc-pVDZ	5.30
P2	PW91	ΔSCF	pw	5.08
P2	PW91	SJ-TS	pw	5.10
P2	B3LYP	ΔSCF	6–31g(d)	5.35
P2	B3LYP	ΔSCF	cc-pVDZ	4.91
P2	HSE06	ΔSCF	6–31g(d)	5.33
P2	HSE06	ΔSCF	cc-pVDZ	4.88

O1/P1. For many molecular systems, a near cancellation of electronic self-energy and electron-hole attraction effects is observed, which often allows for a meaningful description of the molecular optical response already on the IPA level of theory. This is clearly not the case for the present systems, where many-body effects lead to dramatic changes in the calculated optical spectra. In case of O1, not only a strong blueshift of the optical absorption is observed in the TDDFT calculations, but also the line shape changes and two rather than one pronounced absorption peaks appear. TDDFT based on PW91/B3LYP in the adiabatic approximation yields two peaks at around 3.5/3.8 and 4.5/5.0 eV for O1. The corresponding calculations for P1 give rise to a single pronounced peak at about 3.5/3.6 eV. The transition orbitals contributing to these peaks were determined using natural transition orbital (NTO) analysis[98] and are shown in Figure 7. They are in agreement with the orbitals identified in earlier studies.[6,16]

Alternatively, we calculate the optical response from the BSE based on QP corrections obtained from G_0W_0 calculations and the PW91 wave functions. As already found in earlier studies on molecular systems, see, e.g., Ref. [63], the inclusion of local-field effects is essential for the calculation of meaningful excitation energies. It blueshifts the excitation energies by more than one eV. Smaller, but still noticeable is the effect of the resonant-nonresonant coupling terms: Calculations performed within the Tamm-Dancoff approximation (BSE-TDA) result in larger excitation energies than calculations performed using the full exciton Hamiltonian (BSE), as shown in Figure 6. We notice that the effect of the resonant-nonresonant coupling is particularly important for the P core, where it redshifts the excitation energies by about 0.5 eV. Comparing TDDFT and BSE spectra of $[Cu_2(en)_2O_2]^{2+}$, one finds a relatively close agreement with respect to both line shapes and relative peak positions. The absolute peak positions deviate from the TDDFT results by a few tenths of an eV, which corresponds to the scatter among the TDDFT results obtained with different XC functionals.

In Figure 8, the optical response of O2 and P2 ($[Cu_2(dbdmed)_2O_2]^{2+}$) calculated within TDDFT is shown. The size of these molecules does not allow for GW-BSE calculations. The calculated optical response of O2 and P2 is rather similar to that of O1 and P1 ($[Cu_2(en)_2O_2]^{2+}$). However, the main absorption features are redshifted by 0.8/1.5 and 0.9 eV, respectively, for the two O and one P transition. In addition to calculations for fully relaxed structures we also present spectra obtained for fixed geometries determined using B3LYP cc-pVDZ calculations. The comparison of the various spectra

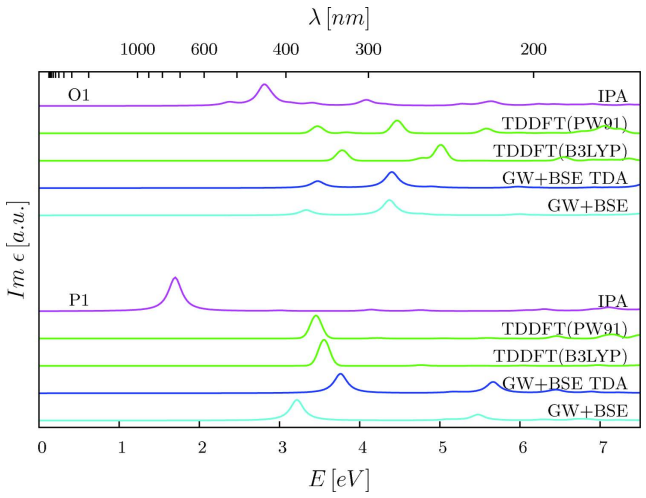

Figure 6. Calculated optical response of O1, P1 ($[Cu_2(en)_2O_2]^{2+}$) calculated with the IPA, TDDFT, and the BSE (see text). [Color figure can be viewed in the online issue, which is available at wileyonlinelibrary.com.]

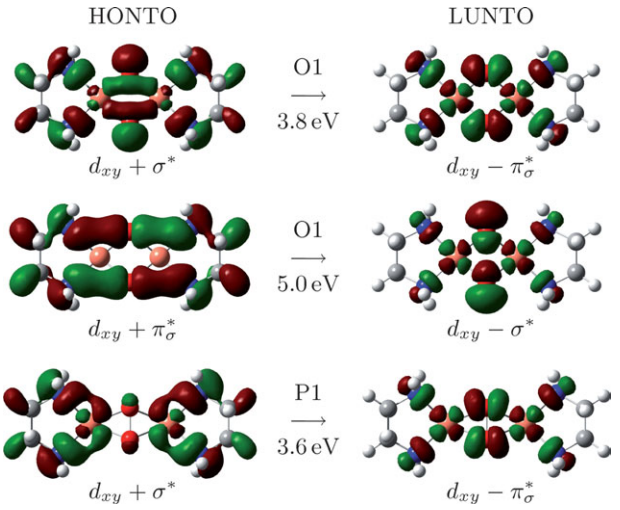

Figure 7. NTO analysis of the relevant O1 and P1 peaks. Shown are the highest occupied transition orbital (HONTO) and the lowest unoccupied transition orbitals (LUNTO). Every pair of orbitals contributes with more than 90% to the corresponding transition.

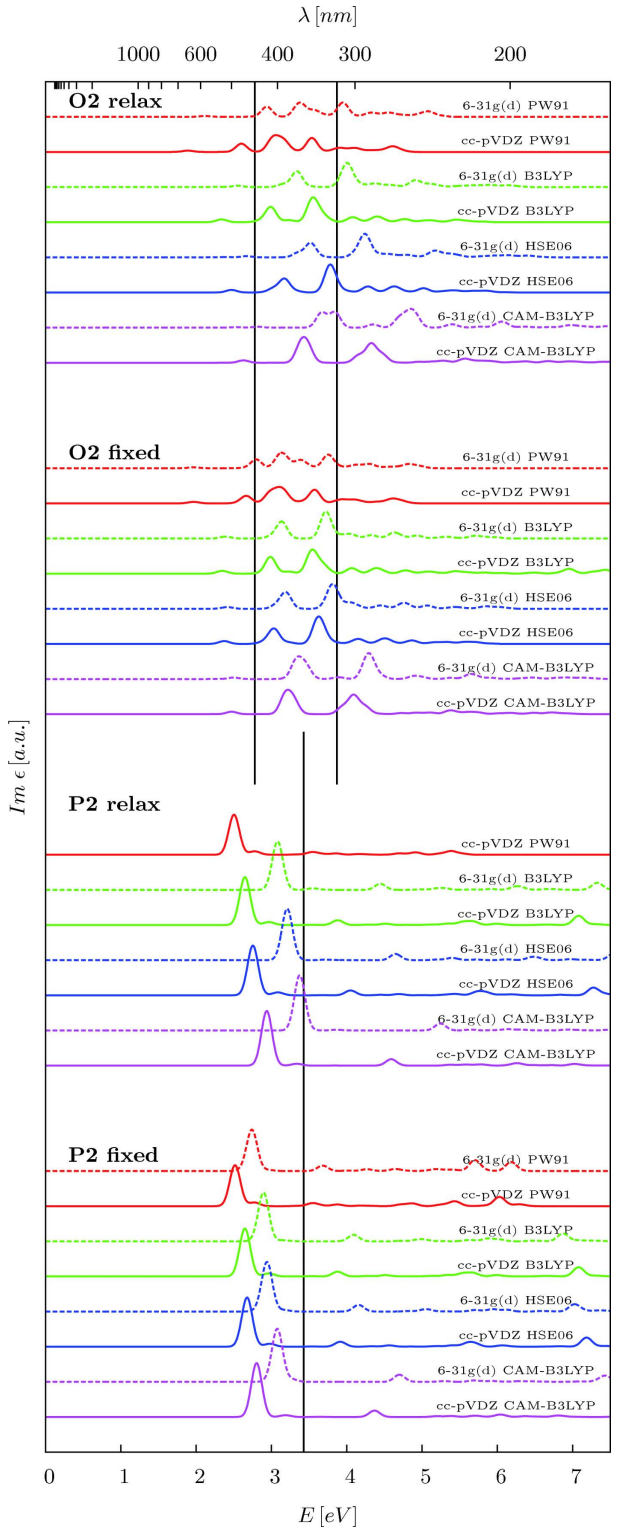

Figure 8. TDDFT spectra (see text) of $[Cu_2(dbdmed)_2O_2]^{2+}$. The vertical lines indicate the experimental absorption peaks from Ref. [97]. [Color figure can be viewed in the online issue, which is available at wileyonlinelibrary.com.]

shows that the basis set, the XC functional, and the geometrical details influence the calculated optical response to a similar degree, by several tenths of an eV.

The measured data from Ref. [99] are also indicated in Figure 8. It is clearly seen that calculations based on local XC functionals underestimate the onset of the optical absorption, while the inclusion of EEX in many cases leads to too large excitations energies. In particular it is found that no combination of a specific functional and basis set describes the O2 and P2 spectra with similar accuracy. While, e.g., CAM-B3LYP in conjunction with the 6-31g(d) basis describes the experiment well for P2, the same theoretical treatment of O2 overestimates the optical absorption energies by more than one eV.

In order to investigate to what extent the deviations between experiment and theory may be attributed to solvent effects, we performed additional calculations. In case of the plane-wave calculations and using the continuum model described above, we find the THF-induced shifts of the optical absorption peaks to be below 0.05 and 0.1 eV for O1 and P1, respectively. Solvent cavity reaction field calculations with localized basis sets for $[Cu_2(en)_2O_2]^{2+}$ show only a small dependence of the structural and electronic properties on the relative permittivity of the solvent. Even water, the solvent with the highest permittivity tested, leads to maximum distance changes ΔCu—Cu/ΔO—O/ΔCu—N for O1, P1 of 0.034/−0.025/−0.014, 0.007/−0.015/−0.012 Å. The optical absorption features of O1/P1 are red shifted 0.03/0.15 eV. Obviously, the solvent-related effects on optical absorption energies are far smaller than, e.g., differences due to the usage of different XC functionals within the TDDFT. This is not related to the usage of the continuum models in the theoretical description, as confirmed by test calculations, where up to four weakly coordinating solvent acetonitril molecules were explicitly taken into account: Two different stable configurations positions were probed, coordinating directly a copper atom with nitrogen or forming a hydrogen bond between nitrogen and copper. From the energetic point of view, the latter configuration is favored. Unsymmetrical coupling of solvent molecules leads to peak splitting of the order of 0.2 eV. Symmetric coordination shifts the spectra by about 0.1 eV.

Conclusions

The structural, electronic, and optical properties of $[Cu_2(dbdmed)_2O_2]^{2+}$ and $[Cu_2(en)_2O_2]^{2+}$ have been calculated from *first principles*. Concerning the spin structure of the ground state, we find for the O structure the spin singlet to be energetically preferred, while the results for the P core depend on the specific XC functional used in the calculations. In particular, hybrid functionals tend to favor the singlet state less than (semi)local functionals compared to the triplet. The influence of the EEX amount in the XC functional on the energy comparison between O and P structures is found to depend on the basis set. In the case of cc-pVDZ calculations, EEX seems to favor the P core, while the opposite occurs for 6-31g(d). Also, the structural details of the O and P core depend on basis set and XC functional used in the calculation. We find the O—O/Cu—Cu distance in the O core of $[Cu_2(dbdmed)_2O_2]^{2+}$ to vary between 2.24/2.75 and 2.31/2.89 Å. The corresponding values for the P core are 1.43/3.44 and 1.50/3.63 Å. Similar values are obtained for $[Cu_2(en)_2O_2]^{2+}$, with slightly larger O—O and corresponding shorter Cu—Cu distances for the O core. The calculated HOMO-LUMO gaps increase

strongly (from about 1 to 6 eV in case of the O structure of $[Cu_2(dbdmed)_2O_2]^{2+}$) with the amount of EEX in the XC functional. Also, the energy ordering of the molecular states is strongly affected by the XC functional. The dependence on the XC functional is reduced in the QP gaps. Irrespective of whether they are calculated from the G_0W_0 approach or using occupation constrained DFT, a value of about 5 eV marks the lower limit of the QP gap for both $[Cu_2(dbdmed)_2O_2]^{2+}$ and $[Cu_2(en)_2O_2]^{2+}$. In comparison to the single-particle gaps calculated within DFT-PW91, this corresponds to electronic self-energy effects of the order of about 4 eV. Thereby we observe the trend that semilocal functionals such as PW91 predict larger QP gaps for P than for O, while the trend is reversed for calculations based on hybrid functionals. The calculated optical response is strongly affected by many-particle effects. This concerns both the peak shapes and the energy positions. TDDFT calculations and the Bethe-Salpeter approach lead thereby to qualitatively similar spectra for $[Cu_2(en)_2O_2]^{2+}$. Electron-hole attraction effects of about 2…3 eV are found, and a strong influence of local-field effects and resonant-nonresonant coupling terms is observed. In the case of $[Cu_2(dbdmed)_2O_2]^{2+}$ where measured optical absorption data are available, it is found that the TDDFT calculations describe the essential features of the experiment correctly but show a large scatter with respect to the influence of the basis set and the XC functional used in the adiabatic approximation. The agreement with experiment is best if B3LYP and CAM-B3LYP in conjunction with a 6-31g(d) basis are used for O and P, respectively. None of the XC functionals probed here within TDDFT does particularly well for *all* molecular systems investigated.

In fact, altogether our work supports earlier findings by Gherman and Cramer that "different functionals are required for accuracy in different regions of the potential energy surface". While this is not satisfactory, the present work demonstrates, on the other hand, that meanwhile relatively complex molecules can be modeled realistically using many-body perturbation theory approaches. It is our hope that the application of such methods in conjunction with complete and orthogonal basis sets—ideally with better approximations to the molecular screening—will help to shed more light on the remaining ambiguities.

Acknowledgments

We thank Jean-Luc Fattebert for helping us with the implementation of the continuum solvent model in the plane-wave code. The calculations were performed by using grants of the Höchstleistungs-Rechenzentrum Stuttgart and the Paderborn Center for Parallel Computing PC².

Keywords: DFT · TDDFT · GWA · BSE · optical absorption

How to cite this article: M. Rohrmüller, S. Herres-Pawlis, M. Witte, WG. Schmidt, *J. Comput. Chem.* **2013,** *34,* 1035–1045. DOI: 10.1002/jcc.23230

[1] E. I. Solomon, U. M. Sundaram, T. E. Machonkin, *Chem. Rev.* **1996**, *96,* 2563.
[2] Y. Matoba, T. Kumagai, A. Yamamoto, H. Yoshitsu, M. Sugiyama, *J. Biol. Chem.* **2006**, *281,* 8981.
[3] H. Decker, T. Schweikardt, F. Tuczek, *Angew. Chem. Int. Ed.* **2006**, *45,* 4546.
[4] K. D. Karlin, Z. Tyeklar, Eds. Bioinorganic Chemistry of Copper; Chapman and Hall: New York, **1993**.
[5] N. Kitajima, Y. Moro-Oka, *Chem. Rev.* **1994**, *94,* 737.
[6] L. M. Mirica, X. Ottenwaelder, T. D. P. Stack, *Chem. Rev.* **2004**, *104,* 1013.
[7] T. D. P. Stack, *Dalton Trans.* **2003**, *10,* 1881.
[8] K. A. Magnus, H. Ton-That, J. E. Carpenter, *Chem. Rev.* **1994**, *94,* 727.
[9] K. A. Magnus, B. Hazes, H. Ton-That, C. Bonaventura, J. Bonaventura, W. G. L. Hol, *Protein Struct. Funct. Bioinformatics* **1994**, *19,* 302.
[10] M. Rolff, J. Schottenheim, H. Decker, F. Tuczek, *Chem. Soc. Rev.* **2011**, *40,* 4077.
[11] R. R. Jacobson, Z. Tyeklar, K. D. Karlin, S. Liu, J. Zubieta, *J. Am. Chem. Soc.* **1988**, *110,* 3690.
[12] A. G. Blackman, W. B. Tolman, *Struct. Bond.* **2000**, *97,* 179.
[13] E. A. Lewis W. B. Tolman, *Chem. Rev.* **2004**, *104,* 1047.
[14] J. A. Halfen, S. Mahapatra, E. C. Wilkinson, S. Kaderli, V. G. Young, Jr., L. Que, Jr., A. D. Zuberbühler, W. B. Tolman, *Science* **1996**, *271,* 1397.
[15] C. J. Cramer, M. Wloch, P. Piecuch, C. Puzzarini, L. Gagliardi, *J. Phys. Chem. A* **2006**, *110,* 1991.
[16] M. J. Henson, P. Mukherjee, D. E. Root, T. D. P. Stack, E. I. Solomon, *J. Am. Chem. Soc.* **1999**, *121,* 10332.
[17] L. M. Mirica, M. Vance, D. J. Rudd, B. Hedman, K. O. Hodgson, E. I. Solomon, T. D. P. Stack, *Science* **2005**, *308,* 1890.
[18] J. L. Lewin, D. E. Heppner, C. J. Cramer, *J. Biol. Inorg. Chem.* **2007**, *12,* 1221.
[19] B. F. Gherman, C. J. Cramer, *Coord. Chem. Rev.* **2009**, *253,* 723.
[20] P. E. M. Siegbahn, M. Wirstam, *J. Am. Chem. Soc.* **2001**, *123,* 11819.
[21] P. E. M. Siegbahn, *J. Biol. Inorg. Chem.* **2003**, *8,* 577.
[22] P. E. M. Siegbahn, *J. Biol. Inorg. Chem.* **2006**, *11,* 695.
[23] M. Güell, P. E. M. Siegbahn, *J. Biol. Inorg. Chem.* **2007**, *12,* 1251.
[24] P. E. M. Siegbahn, M. R. A. Blomberg, *J. Phys. Chem. A* **2008**, *112,* 12772.
[25] B. T. Op't Holt, M. A. Vance, L. M. Mirica, D. E. Heppner, T. D. P. Stack, E. I. Solomon, *J. Am. Chem. Soc.* **2009**, *131,* 6421.
[26] A. Poater, L. Cavallo, *Inorg. Chem.* **2009**, *48,* 4062.
[27] T. Saito, Y. Kataoka, Y. Nakanishi, T. Matsui, Y. Kitagawa, T. Kawakami, M. Okumura, K. Yamaguchi, *Int. J. Quantum Chem.* **2009**, *109,* 3649.
[28] Y. Takano, K. Koizumi, H. Nakamura, *Inorg. Chim. Acta* **2009**, *362,* 4578.
[29] M. Güell, J. M. Luis, M. Sola, P. E. M. Siegbahn, *J. Biol. Inorg. Chem.* **2009**, *14,* 229.
[30] T. Saito, Y. Kataoka, Y. Nakanishi, T. Matsui, Y. Kitagawa, T. Kawakami, M. Okumura, K. Yamaguchi, *Chem. Phys.* **2010**, *368,* 1.
[31] S. Herres-Pawlis, P. Verma, R. Haase, P. Kang, C. T. Lyons, E. C. Wasinger, U. Flörke, G. Henkel, T. D. P. Stack, *J. Am. Chem. Soc.* **2009**, *131,* 1154.
[32] P. Kang, E. Bobyr, J. Dustman, K. O. Hodgson, B. Hedman, E. I. Solomon, T. D. P. Stack, *Inorg. Chem.* **2010**, *49,* 11030.
[33] D. G. Liakos, F. Neese, *J. Chem. Theor. Comput.* **2011**. *7,* 1511.
[34] F. Neese, *J. Biol. Inorg. Chem.* **2006**, *11,* 702.
[35] M. F. Rode, H.-J. Werner, *Theor. Chem. Acc.* **2005**, *114,* 309.
[36] M. Flock, K. Pierloot, *J. Phys. Chem. A* **1999**, *103,* 95.
[37] P. E. M. Siegbahn, *Faraday Discuss.* **2003**, *124,* 289.
[38] F. Neese, D. G. Liakos, S. Ye, *J. Biol. Inorg. Chem.* **2011**, *16,* 821.
[39] G. Onida, L. Reining, A. Rubio, *Rev. Mod. Phys.* **2002**, *74,* 601.
[40] T. Stein, L. Kronik, R. Baer, *J. Am. Chem. Soc* **2009**, *131,* 2818.
[41] P. Dev, S. Agrawal, N. J. English, *J. Chem. Phys.* **2012**, *136,* 224301.
[42] R. M. Dreizler, E. K. U. Gross, Density Functional Theory; Springer-Verlag: Berlin, **1990**.
[43] M. Preuss, W. G. Schmidt, K. Seino, J. Furthmüller, F. Bechstedt, *J. Comput. Chem.* **2004**, *25,* 112.
[44] A. Hermann, W. G. Schmidt, P. Schwerdtfeger, *Phys. Rev. Lett.* **2008**, *100,* 207403.
[45] T. Kowalczyk, S. R. Yost, T, van Voorhis, *J. Chem. Phys.* **2011**, *134,* 054128.
[46] L. Hedin, *Phys. Rev.* **1965**, *139,* A769.

[47] L. Hedin, S. Lundqvist, In Solid State Physics, Vol. *23; H. Ehrenreich, F. Seitz, D. Turnball, Eds.; Academic, New York,* **1969**; p. 1.
[48] M. S. Hybertsen, S. G. Louie, *Phys. Rev. B* **1986**, *34,* 5390.
[49] F. Bechstedt, In Festkörperprobleme/Advances in Solid State Physics, Vol. *32; U. Rössler, Ed.; Vieweg, Braunschweig/Wiesbaden,* **1992**; p. 161.
[50] F. Aryasetiawan, O. Gunnarsson, *Rep. Prog. Phys.* **1998**, *61,* 237.
[51] W. G. Aulbur, L. Jonsson, J. W. Wilkins, In Solid State Physics: Advances in Research and Applications, Vol. *54; H. Ehrenreich, F. Spaepen, Ed.; Academic, San Diego,* **2000**; p. 1.
[52] M. Rohlfing, S. G. Louie, *Phys. Rev. Lett.* **1998**, *80,* 3320.
[53] W. G. Schmidt, S. Glutsch, P. H. Hahn, F. Bechstedt, *Phys. Rev. B* **2003**, *67,* 085307.
[54] S. Albrecht, L. Reining, R. DelSole, G. Onida, *Phys. Rev. Lett.* **1998**, *80,* 4510.
[55] L. X. Benedict, E. L. Shirley, R. B. Bohn, *Phys. Rev. Lett.* **1998**, *80,* 4514.
[56] W. G. Schmidt, M. Albrecht, S. Wippermann, S. Blankenburg, E. Rauls, F. Fuchs, C. Rödl, J. Furthmüller, A. Hermann, *Phys. Rev. B* **2008**, *77,* 035106.
[57] M. Rohlfing, S. G. Louie, *Phys. Rev. Lett.* **1999**, *83,* 856.
[58] P. H. Hahn, W. G. Schmidt, F. Bechstedt, *Phys. Rev. Lett.* **2001**, *88,* 016402.
[59] K. Hummer, C. Ambrosch-Draxl, G. Bussi, A. Ruini, M. J. Caldas, E. Molinari, R. Laskowski, N. E. Christensen, *phys. Stat. Sol. B* **2005**, *242,* 1754.
[60] P. H. Hahn, W. G. Schmidt, K. Seino, M. Preuss, F. Bechstedt, J. Bernholc, *Phys. Rev. Lett.* **2005**, *94,* 037404.
[61] P. H. Hahn, W. G. Schmidt, F. Bechstedt, *Phys. Rev. B* **2005**, *72,* 245425.
[62] Y. Ma, M. Rohlfing, C. Molteni, *Phys. Rev. B* **2009**, *80,* 241405.
[63] C. Ambrosch-Draxl, D. Nabok, P. Puschnig, C. Meisenbichler, *New J. Phys.* **2009**, *11,* 125010.
[64] J. M. Garcia-Lastra, K. S. Thygesen, *Phys. Rev. Lett* **2011**, *106,* 187402.
[65] X. Blase, C. Attaccalite, *Appl. Phys. Lett.* **2011**, *99,* 171909.
[66] A. Riefer, E. Rauls, W. G. Schmidt, J. Eberhard, I. Stoll, J. Mattay, *Phys. Rev. B* **2012**, *85,* 165202.
[67] A. M. Conte, L. Guidoni, R. Del Sole, O. Pulci, *Chem. Phys. Lett.* **2011**, *515,* 290.
[68] B. Baumeier, D. Andrienko, Y. Ma, M. Rohlfing, *J. Chem. Theory Comput.* **2012**, *8,* 997.
[69] B. Baumeier, D. Andrienko, M. Rohlfing, *J. Chem. Theory Comput.* **2012**, *8,* 2790.
[70] E. K. Chang, E. L. Shirley, Z. H. Levine, *Phys. Rev. B* **2001**, *65,* 035205.
[71] R. Leitsmann, W. G. Schmidt, P. H. Hahn, F. Bechstedt, *Phys. Rev. B* **2005**, *71,* 195209.
[72] J. P. Perdew, J. A. Chevary, S. H. Vosko, K. A. Jackson, M. R. Pederson, D. J. Singh, C. Fiolhais, *Phys. Rev. B* **1992**, *46,* 6671.
[73] J. Heyd, G. E. Scuseria, M. Ernzerhof, *J. Chem. Phys.* **2003**, *118,* 8207.
[74] C. Lee, W. Yang, R. G. Parr, *Phys. Rev. B* **1988**, *37,* 785.
[75] A. D. Becke, *J. Chem. Phys.* **1993**, *98,* 5648.
[76] A. D. Becke, *J. Comput. Chem.* **1999**, *20,* 63.
[77] T. Yanai, D. P. Tew, N. C. Handy, *Chem. Phys. Lett.* **2004**, *393,* 51.
[78] G. Kresse, J. Furthmüller, *Comput. Mater. Sci.* **1996**, *6,* 15.
[79] M. J. Frisch, G. W. Trucks, H. B. Schlegel, G. E. Scuseria, M. A. Robb, J. R. Cheeseman, G. Scalmani, V. Barone, B. Mennucci, G. A. Petersson, H. Nakatsuji, M. Caricato, X. Li, H. P. Hratchian, A. F. Izmaylov, J. Bloino, G. Zheng, J. L. Sonnenberg, M. Hada, M. Ehara, K. Toyota, R. Fukuda, J. Hasegawa, M. Ishida, T. Nakajima, Y. Honda, O. Kitao, H. Nakai, T. Vreven, J. A. Montgomery, Jr., J. E. Peralta, F. Ogliaro, M. Bearpark, J. J. Heyd, E. Brothers, K. N. Kudin, V. N. Staroverov, R. Kobayashi, J. Normand, K. Raghavachari, A. Rendell, J. C. Burant, S. S. Iyengar, J. Tomasi, M. Cossi, N. Rega, J. M. Millam, M. Klene, J. E. Knox, J. B. Cross, V. Bakken, C. Adamo, J. Jaramillo, R. Gomperts, R. E. Stratmann, O. Yazyev, A. J. Austin, R. Cammi, C. Pomelli, J. W. Ochterski, R. L. Martin, K. Morokuma, V. G. Zakrzewski, G. A. Voth, P. Salvador, J. J. Dannenberg, S. Dapprich, A. D. Daniels, Ö. Farkas, J. B. Foresman, J. V. Ortiz, J. Cioslowski, D. J. Fox, Gaussian 09 Revision B01; Gaussian Inc: Wallingford, CT; **2009**.
[80] P. E. Blöchl, *Phys. Rev. B* **1994**, *50,* 17953.
[81] G. Kresse, D. Joubert, *Phys. Rev. B* **1999**, *59,* 1758.
[82] J. Tomasi, B. Mennucci, R. Cammi, *Chem. Rev.* **2005**, *105,* 2999.
[83] J. L. Fattebert, F. Gygi, *Int. J. Quantum Chem.* **2003**, *93,* 139.
[84] O. Andreussi, I. Dabo, N. Marzari, *J. Chem. Phys.* **2012**, *136,* 064102.
[85] M. Shishkin, G. Kresse, *Phys. Rev. B* **2006**, *74,* 035101.
[86] R. E. Stratman, G. E. Scuseria, M. J. Frisch, *J. Chem. Phys.* **1998**, *109,* 8218.
[87] G. Scalmani, M. J. Frisch, B. Mennucci, J. Tomasi, R. Cammi, V. Barone, *J. Chem. Phys.* **2006**, *124,* 094107.
[88] H. Ehrenreich, M. H. Cohen, *Phys. Rev.* **1959**, *115,* 786.
[89] S. L. Adler, *Phys. Rev.* **1962**, *126,* 413.
[90] N. Wiser, *Phys. Rev.* **1963**, *129,* 62.
[91] M. Gajdos, K. Hummer, G. Kresse, J. Furthmüller, F. Bechstedt, *Phys. Rev. B* **2006**, *73,* 045112.
[92] V. Olevano L. Reining, *Phys. Rev. Lett.* **2001**, *86,* 5962.
[93] F. Bechstedt, R. Del Sole, G. Cappellini, L. Reining, *Solid State Commun.* **1992**, *84,* 765.
[94] A. Riefer, F. Fuchs, C. Rödl, A. Schleife, F. Bechstedt, R. Goldhahn, *Phys. Rev. B* **2011**, *84,* 075218.
[95] F. Fuchs, C. Rödl, A. Schleife, F. Bechstedt, *Phys. Rev. B* **2008**, *78,* 085103.
[96] A. Ruini, M. J. Caldas, G. Bussi, E. Molinari, *Phys. Rev. Lett.* **2002**, *88,* 206403.
[97] M. Grüning, A. Marini, X. Gonze, *Nano Lett.* **2009**, *9,* 2820.
[98] R. L. Martin, *J. Chem. Phys.* **2003**, *118,* 4775.
[99] V. Mahadevan, M. J. Henson, E. I. Solomon, T. D. P. Stack, *J. Am. Chem. Soc.* **2000**, *122,* 10249.

Received: 18 October 2012
Revised: 13 December 2012
Accepted: 14 December 2012
Published online on 8 January 2013